Human Movement Sciences: Sport, Exercise & Health (research)

Research Internship Research Master 2012-2013

Hubness and synchronisation of scale-free coupled phase oscillators and the relation to neurodegenerative diseases

VU University Amsterdam
Faculty of Human Movement Sciences
Qualification: MSc in Human Movement Sciences
Research Internship Research Master
Author: F.M.T. Coopmans
Supervisor: prof. dr. A. Daffertshofer
October 2013

Abstract

Disease severity of the seminal neurodegenerative diseases including Alzheimer's disease (AD) and Parkinson's disease (PD) is associated with a progressive disruption of functional brain activity as compared to the healthy brain. Recent studies have reported a significant role of cortical hubs in this observed altered brain activity, e.g. hubs are targeted which thereby affects the brain network and its phase synchronisability in AD. However, the effect of the number of hubs in networks with respect to network dynamics, e.g. synchronisation, is poorly understood. In this study I present a preferential rewiring method to increase the number of hubs in a sparse non-growing network of coupled Kuramoto phase oscillators; the latter represents oscillatory activity in distinct brain regions. To gain insight into the effect of (changes in) the number of hubs, quantified through hubness H, on network synchronisability, quantified through phase divergence r, I adopted a system identification approach. I found that H has a profound positive effect on network synchronisability and hubness is a requisite to obtain global phase synchronisation in sparse networks. Furthermore, for low-to-medium H I observed a critical transient regime of locally stable modes of partial synchronisation, indicating that hubness is a critical factor in inducing multistability. These results suggest that in sparse networks such as the functional brain an optimal hubness exists with respect to the maximal functional repertoire and any deviation from this optimum could have great impact on the multistability of the network. To test its validity on empirical data I applied the same approach to resting-state MEG times-series of PD patients. Although my numerical simulations appear clear-cut predictors of effects of hubness in synchronisation networks, the application on the PD data should be considered preliminary. While in its infancy, I do consider my approach a promising future diagnostic and predictive tool.

Key words

Introduction

Functional networks of the human brain cortex are typically defined through synchronisation patterns. This is of specific interest because synchronisation of brain activity appears to alter due to neurodegenerative diseases (NDDs) [1]. Seminal examples of this are altered oscillatory activity, e.g. disturbing synchronisation between neural populations, in Alzheimer's disease (AD) and Parkinson's disease (PD). For example, Stoffers and co-workers demonstrated an increase in functional connectivity in early-stage PD resting-state brain activity in the lower alpha band (8-10 Hz) [2]. The more progressed PD patients displayed increased functional connectivity in neighbouring frequency bands. Additionally the severity of Parkinsonism appeared positively associated with theta (4-8 Hz) and beta (13-30 Hz) functional connectivity measures. Another study by the same research group revealed widespread slowing of brain activity of early-stage PD compared to healthy controls [3]. They hypothesised that brain activity could be linked to the topographical pattern of disease progression. Based on similar findings, Wu and co-workers [4] suggested that the disrupted pattern of functional connectivity found in PD patients is related to disease severity. Rather than only being considered in terms of deep- and midbrain dysfunction, PD should hence be regarded as a disconnection syndrome as already suggested by Cronin-Golomb [5]. These results suggest that the observed disrupted brain activity in PD could have its origin in pathology-induced topological changes in the brain. However, cause-and-effect of altered network topology of the brain and its disrupted oscillatory activity remains unknown.

Several studies in patients with AD revealed distinctive brain activity. For instance, Greicius and co-workers reported decreased resting-state activity in AD patients in specific regions, thereby distinguishing AD from changes observed in healthy aging [6]. Stam and co-workers [7] found that AD is also characterised by a loss of small-world network characteristics such as an increased path length. Other studies from the latter research group [7-9] addressed resting-state data using graph theoretical measures unravelling disruptions of large-scale brain activity, where the disruptions in the lower alpha band (8-10 Hz) were suggested to be caused by targeted attacks on the network's major hubs [9]. This advocates the characterisation of AD as a 'disconnection syndrome' [10-11]. In fact it even goes beyond the mere disconnection by specifying highly connected targets, i.e. hubs, which are more likely to be hit by the disease. This could suggest that disrupted brain activity as found in AD is a result of the targeting of regions central to the brain network.

In epilepsy another role of hubs in the brain network has been reported. Morgan and co-workers [12] revealed that an increase rather than a decrease in neural hubs might be the cause of epileptic seizures. Zhang and co-workers further supported these results by revealing increased nodal characteristics in brain regions affected in epilepsy [13]. They suggested that disruption in the functional and structural brain network in epilepsy may be explained by abnormal hub properties in the affected regions.

Is the targeting of regions central to the brain network, i.e. alterations in the number of hubs, able to explain disrupted brain activity? Additionally one may ask whether the disruption of hubs is a more general neurodegenerative process characteristic of NDDs in general. Neural hubs are considered to be crucial in normal brain functioning since they connect large areas of the brain and increase information transfer between areas. However, to the best of my knowledge the exact influence of variation in the number of hubs (i.e. hub vulnerability or increases in hubs) on brain activity is unknown.

To gain insight into the effect of the number of hubs in brain networks on its dynamics (e.g., phase synchronisability) in a controlled setting these networks can be modelled. A simple but successful model to study global synchronisation of networks is the Kuramoto model [14-15], where a phase oscillator represents each member of the network. This allows for a detailed study of the influence of characteristics of these networks on phase synchronisation. For example, the distribution of native frequencies of oscillators [16], modularity [17], regular [18-19], small-world [20-22] and scale-free networks [23-24].

Hong and co-workers [22] induced a rewiring paradigm to examine the synchronisability of evolving small-world networks using a fixed probability p. Small-world networks, however, are not prone to induce hubs and to date the specific effects of the number of hubs in networks with respect to network dynamics, e.g., synchronisation, are poorly understood. To increase the number of hubs in a network a scale-free topology as first described by Barabasi and Albert [25] has to be induced. This model induces a scale-free network by adding nodes with connections dependent on the degree of the existing

nodes, i.e. so-called preferential attachment. While nodes are added, highly connected nodes (hubs) are more likely to be attached to new nodes. A downside of this model, however, is that the scale-free topology is induced by growth, whereas developed brain networks generally do not exhibit an increase in brain regions. Park and co-workers revealed that the growth characteristic is not necessary for complex networks to self-organise into a scale-free state [26]. Since then, these non-growing preferential rewiring networks [26-28] have only received modest attention in literature. However, they offer a solid solution for the proposed problems arising in growing networks.

In the first part of the current study I present a preferential rewiring approach based on the combined methods proposed by Hong and co-workers [22] and Xie and co-workers [27] to increase the number of hubs, i.e. hubness H, in a sparse non-growing network of coupled Kuramoto phase oscillators; the latter is here considered to represent oscillatory activity in distinct brain regions. By combining network (graph) theory with non-linear dynamics (here the Kuramoto model) theoretical estimates are achieved to quantify the effect of H on the (stability of) synchronisation of phase oscillators. I adopted the phase divergence or order parameter r as a measure of global synchronisation. To gain further insight into the effects of changes in hubness H on network dynamics I used a system identification approach based on the estimation of Kramers-Moyal coefficients, as first proposed by Friedrich and Peinke [29]. Here I hypothesised that an initial increase in hubness is beneficial for network synchronisation. A general characteristic of hubs is that they cause a decrease in characteristic path length [30], which enhances the transition to the synchronisation state [22]. Furthermore, hubs cause local structures to become increasingly connected into modules and this could cause local synchronisation within these different hub modules to occur on a fast time scale whereas global synchronisation is hampered. As hubness increases further, hubs are more likely to be directly interconnected into so-called rich-clubs [31]. Low-degree nodes could become excluded from these modules and would thereby halter global synchronisation [32]. I thus expected the evolving network to exhibit different optimal hubness with respect to local synchronisability where different semi-stable states of partial synchronisation co-exist on the one hand and global (full) synchronisation on the other hand.

The overarching objective of this study was to find generic (organisational) principles in neurodegenerative diseases, where I wondered if the characteristics found in AD and epilepsy, i.e. hub vulnerability and increases of hubs respectively, are a general neurodegenerative process characteristic of NDDs. In the second part of this study the simulated results were qualitatively compared with resting-state brain activity (MEG) of PD patients [2-3]. Studies previously mentioned highlight that in the neurodegenerative brain hubs could be a target of alterations, i.e. degenerative attack or growth. Since it has been suggested that the human brain is optimised by evolutionary principles [33], I expected the human brain to possess a optimal number of hubs. I thus hypothesised that NDDs can be more generally characterised by a sub-optimal hubness and more specific that hub vulnerability is also present in resting-state PD. To examine hubness in brain networks in more detail a system identification approach prone to detecting differences in synchronisability and synchronisation dynamics was employed. The main focus of the second part of the study was to validate the applicability of this unbiased system identification approach to resting-state MEG time-series.

3

Methods part I

Scale-free Kuramoto model

The Kuramoto model [14] of coupled phase oscillators has a wide range of applications and is frequently used in neurobiological models due to its seminal form and analytic capacity for describing synchronous behaviour. Here I considered a stochastic Kuramoto network of N coupled non-identical phase oscillators that interact via undirected and unweighted connections according to:

$$\dot{\theta}_i = \omega_i + \xi_i(t) + \frac{K}{N} \sum_j A_{ij} \sin(\theta_j - \theta_i) \,. \tag{1}$$

In this network, the phase of oscillator i is influenced through coupling, determined by global coupling strength K (scaled by the amount of coupled phase oscillators N), with oscillator j, its own natural frequency ω_i and stochastic force $\xi_i(t)$. The stochastic force is white noise induced to perturb the evolution of phases, and can be described by

$$\langle \xi_i(t) \rangle = 0$$
$$\langle \xi_i(t)\xi_j(t') \rangle = 2Q\delta_{ij}\delta(t - t').$$

The angular brackets represent averages over different noise realisations, Q is the noise strength and represents the noise variance, δ_{ij} is the Kronecker delta function excluding noise-correlation between oscillators i and j and $\delta(t - t')$ is the Dirac delta function. The unweighted adjacency matrix A_{ij} is a $N \times N$-matrix and defines the structural coupling between neighbouring oscillators (nodes) i and j, with its binary elements representing the coupling between node i and node j; $A_{ij} = 0$ for disconnected nodes, $A_{ij} = 1$ for connected nodes. For undirected unweighted network the adjacency matrix is symmetric, i.e. $A_{ij} = A_{ji}$ and the node degree k_i, i.e. the number of connections of a node, is given as

$$k_i = \sum_j A_{ij}$$

where the sum is over all nodes of the network.

The networks were modelled to be scale-free, i.e. the node degrees in the network obey a power law distribution. This is thought to reflect the functional connections in the brain as they have been shown to have a scale-free distribution; e.g., [34-36]. Scale-free networks were first described by Barabási and Albert [25] and are characterised by high-degree nodes, from here-on referred to as hubs. Their scale-free network theory incorporates two characteristics of real networks that are not included in the random [37] and small-world [38] network theories: *growth* and *preferential attachment*. Growth is the addition of new nodes and connections to the network; preferential attachment is the non-uniform preference of this addition, i.e. new nodes are more likely to have connections to nodes already having a high number of connections. These two characteristics allow for the emergence of hubs. However, in biological networks like the post-natal human brain, the number of neurons is not (significantly) increasing; structural changes are typically accomplished by altering connections between neurons (or by reducing the number of neurons due to pathology). Regarding modelling, many limitations appear with an increase of the number of nodes N or connections k, such as effects on the degree distribution [39], synchronisation dynamics (see, e.g., [17]) and influences on graph theoretical measures used to define networks [40]. These N, k-dependencies can be avoided by adopting a fixed number of nodes N and fixed average number of connections, i.e. a fixed average node degree

$$\langle k \rangle = \frac{1}{N} \sum_i k_i \,.$$

Additionally, Park et al. [26] have shown that the growth characteristic is not needed for a complex network to self-organise into a scale-free state. Although these non-growing preferential rewiring networks [26-28] only received modest attention in literature, they offer a solid solution for the previously mentioned limitations arising in networks incorporating growth.

Simulations

I adopted the non-growing preferential rewiring network based on the model proposed by Xie and co-workers [27] such that the number of nodes N and average node degree $\langle k \rangle$ was kept constant. I defined the network evolution according to a number of steps (Figure 1):

> 1. *Initial network.* The network started with a fixed number of unweighted nodes N=150 and a fixed degree k=4 (hence 600 connections) in a regular ring lattice network structure. The average node degree was defined as 3% in line with findings

of a brain mapping study of Hagmann and co-workers [41] who investigated large-scale structural brain networks using diffusion spectrum imaging. By definition no hubs were present at start.

2. Rewiring the network. With each rewiring step S a connection between random chosen nodes i and j was rewired to a random chosen node l, thereby ensuring a fixed number of edges. The probability that a connection is rewired from node i to node l depended on the normalised node degree k_l of node l, i.e.

$$P_{i \to l}(k_l) = k_l / \sum_n k_n \tag{2}$$

where the probability distribution $P_{i \to l}(k_l)$ provided the probability that a random chosen node has degree k. A constraint here is that nodes or clusters of nodes may not become disconnected. Rewiring stops at $S = 100$.

3. Implement Kuramoto's dynamics on the network. The functional network was created by embedding each obtained adjacency matrix in a Kuramoto model of phase oscillators (1), where each node in the matrix corresponded to a phase oscillator. Natural frequencies ω_i were randomly selected from a Lorentz distribution with width $\gamma = 0.5$. Initial phases $\theta_{i,0}$ were randomly chosen from the uniform distribution $[0, 2\pi]$.
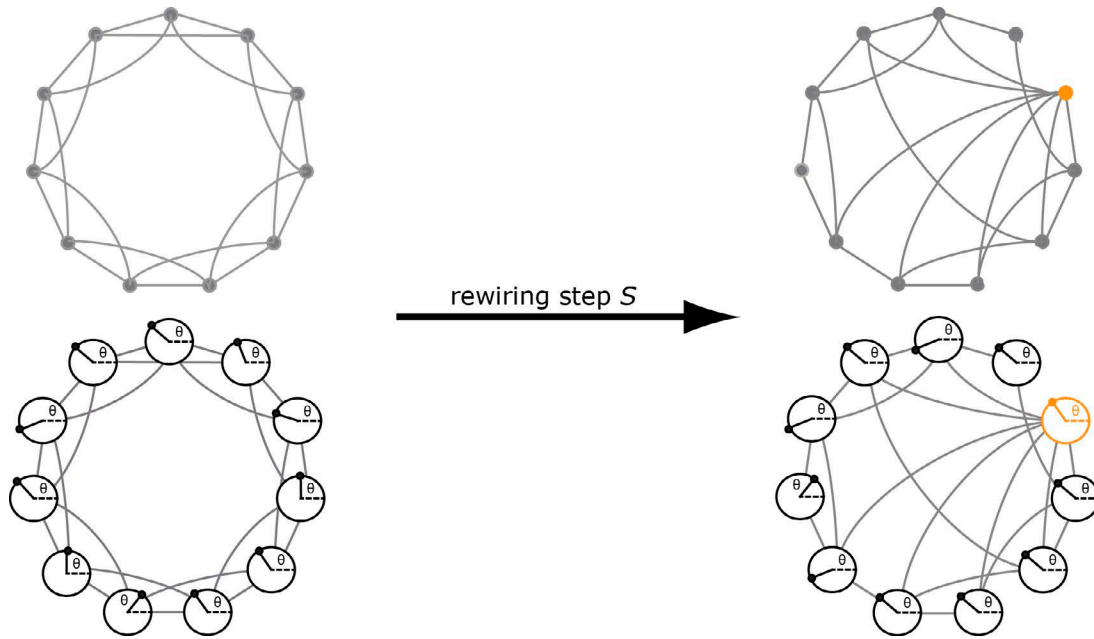
Figure 1 | Example of the non-growing preferential rewiring model embedded in a Kuramoto model of phase oscillators. The initial network was a regular ring lattice (top left graph) with k=4. With rewiring step S connections were preferentially rewired with probability p (top right graph). Each of these evolving network structures was implemented in a Kuramoto model (1)(bottom graphs). In this network one node is quantified as hub node (displayed in orange).

All implemented Kuramoto models were simulated for T subsequent iterations assessing synchronisability of the networks. Pilot simulations revealed increased time duration until steady state was obtained in subcritical regimes ($K < K_c$ and small S). Therefore, the time step between iterations Δt was chosen as $200/T$ with the total number of iterations T set to 10^5. For statistical significance, all simulations were repeated 100 times. Numerical simulations were performed over a range of different positive global coupling $K = [0, 10]$, $\Delta K = 0.1$ as to induce different levels of synchronisation. Simulations were performed for the non-stochastic and stochastic Kuramoto model, i.e. system (1) with $Q = 0$ and $Q = 0.1$, where the stochastic force ξ_i is randomised over time by multiplication with a random normal distribution for each oscillator i. Simulations were performed using a commercial software package (MATLAB 7.14, The Mathworks Inc., Natick, MA, 2000). The preferential attachment method was manually written[1] adopting algorithms from the Systems and Biology Toolbox [42], Matgraph Toolbox [43] and the Brain Connectivity Toolbox [44]. As

---

[1] Matlab source code for the numerical simulations available on request.

a reference Erdös-Rényi networks were simulated with identical topological constraints (i.e., $N = 150$, $\langle k \rangle = 4$) and implemented with the stochastic Kuramoto model, i.e. $Q = 0.1$.

To quantify the number of hubs for all simulated preferential rewiring topologies I adopted both a varying and a fixed hub threshold k_h based on node degree [45]: any node with a degree higher than this threshold was classified as a hub. The varying threshold defined hubs by using a definition based on the variance of node degree and was formally defined as

$$k_h = \langle k \rangle + \sigma,$$

where $\langle k \rangle$ is the aforementioned average node degree and σ the standard deviation of the degree distribution, i.e.:

$$\sigma = \sqrt{\frac{1}{N} \sum_i (k_i - \langle k \rangle)^2}\,.$$

The fixed hub degree used a constant as a threshold to qualify hubs:

$$k_h = C\,,$$

with C=4,5,6. The fixed hub threshold was not influenced by large fluctuations in variance commonly observed in evolving networks as the varying threshold was. After qualifying the number of hubs I defined hubness of the network, i.e. the fraction of nodes with a degree k_i higher than the hub threshold k_h, as

$$H = \frac{1}{N} \sum_i 1 - \Theta(k_h - k_i)\,,$$

with $\Theta(k_h - k_i)$ the Heaviside function such that the sum adds a zero for all nodes having a node degree k_i lower or equal to the hub threshold k_h and a one when higher than this threshold. To validate and explore characteristics of the structural networks evolved using the preferential rewiring method I adopted a number of complex network measures. These include characteristic path length, clustering coefficient, local efficiency, global efficiency, closeness and betweenness centrality. For a more thorough explanation of these (and more) measures please refer to, e.g., [44, 46]. These results are detailed in Appendix A. All necessary implementations to calculate complex network measures were adopted from the Brain Connectivity Toolbox [44].

Analysis
Since the synchronisation behaviour of the network is of interest, the phase divergence or order parameter of the Kuramoto system was calculated according to:

$$r(t) = 1/N \left| \sum_j e^{i\theta_j(t)} \right|, \tag{3}$$

where θ_j was the phase of an oscillator at time t (i.e. iteration n in the simulations). The order parameter r is the **key parameter** in the analysis of the data, since it represents phase coherence and thus the amount of global synchrony in the network. Please note that it can be applied to any data set exhibiting dynamics in the polar plane.

To explore the phase divergence of a system more thoroughly, I used an approach called the extraction procedure, or system identification procedure [47] (see for a more detailed description and possible applications, e.g., [48] or [49]), which has already been applied successfully in a wide variety of topics including turbulent flows [47], economics [50] and rhythmic human movement [51]. This procedure allows for an unbiased method to identify underlying deterministic and stochastic components of complex dynamical systems. Note that the extraction procedure requires the generating processes to exhibit Markov properties. In other words: one has to verify whether the system has no memory. The Kuramoto model of interest is a Markov process since its future state by definition depends on present state only, as presented in Eq. (1). When applying this procedure to other data sets the requirement of Markov properties can be verified by the Chapman-Kolmorogov equation, which reads

$$p(x'', t''|x, t) = \int p(x'', t''|x', t')\, p(x', t'|x, t)\, \mathrm{d}x',$$

where $p(x'', t''|x, t)$ represents the probability density to find a system at state x'' and time t'' when state x and time t are known.

The system under study is a dynamical system, with the order parameter r describing the structure and dynamics of the system. It can be cast in the form of a generalised Langevin-equation

$$\dot{r} = f(r) + g(r)\Gamma(t). \tag{4}$$

This means that I was allowed to describe the evolution of the order parameter (i.e. the derivative of r with respect to time t) as a combination of deterministic ($f(r)$) and stochastic ($g(r)\Gamma(t)$) components. The deterministic components corresponded to the

6

intrinsic forces caused by the interactions between oscillators. The stochastic forces incorporated the randomness of the oscillators' natural frequencies, initial phases and the external noise induced by stochastic force ξ. An estimate of these components was found in terms of the stochastic dynamics' drift and diffusion coefficients $D^{(1)}$ and $D^{(2)}$, which agreed with the first two Kramers-Moyal coefficients in the dynamics of the corresponding probability density [52]. The qth order Kramers-Moyal coefficient was computed according to

$$D^{(q)}(x) = \lim_{\Delta t \to 0} \frac{1}{q!} \frac{1}{\Delta t} \int [x' - x]^q \, p(x', t + \Delta t | x, t) \mathrm{d}x'. \tag{5}$$

The probability density function $p(x', t + \Delta t | x, t)$ represented the probability of the system to obtain state x' at time $t + \Delta t$ after a previous state x at t, where Δt approaches zero. For a numerical estimation of the drift and diffusion coefficients $D^{(1)}$ and $D^{(2)}$ the data was binned[2]. Since the dynamics of r were estimated, the range of values within r was subdivided into equally spaced parts where all repetitions on a fixed value for K and S were taken into account as one long measurement. Each bin was specified by a x value. Then, as Eq. (5) suggests, the probability density function $p(x', t + \Delta t | x, t)$ was determined as follows: when at time t a sample was found in a bin with centre x the probability that the next sample at $t + \Delta t$ will be in a bin with centre x' was calculated. This was carried out for all neighbouring samples and all combinations of bins. The resulting values of the probability function were then multiplied by their corresponding differences raised to the power q ($q = 1$ for the drift coefficient, $q = 2$ for the diffusion coefficient). Subsequently this was integrated over bins of the next sample x' and scaled by $q!$ and time step Δt. Note that the estimation of the drift and diffusion coefficients requires the dynamical system under study to be stationary.

The stochastic differential equation of the order parameter (4) can now be rewritten as

$$\dot{r} = D^{(1)}(r) + \sqrt{2 D^{(2)}(r)} \Gamma(t),$$

where $D^{(1)}$ and $D^{(2)}$ represented the first two Kramers-Moyal coefficients or the drift and diffusion coefficient respectively.

For the sake of brevity, I focused on the deterministic components of network dynamics, i.e. the drift coefficient $D^{(1)}$. This coefficient thus mapped the dynamics of a system without its randomness and thereby identified deterministic attractors and repellers of the system under study. In particular assessing its potential via

$$V\big(D^{(1)}\big) = -\int D^{(1)}(r) \, \mathrm{d}r$$

provided a very accessible way to examine stability of modes of synchronisation, since (local) minima in the potential of $D^{(1)}$ correspond to (local) stable states. To exemplify: if a system exhibited a global minimum in $V(D^{(1)})$ at a certain r, this indicated that the system possessed a global attractor at this value of r such that the system's most stable state was located at this r. Furthermore, local minima in $V(D^{(1)})$ indicated locally stable states.

Statistics
After assessing normality of the outcome parameters I used descriptive statistics in combination with a high number of repetitions of modelling simulations to obtain a distribution of simulated behaviour and average values, variances and confidence intervals of the parameters of interest.

Methods part II

The second part of this study followed the approach to examine characteristics defining network synchronisability as a function of hubness of the previous part (see Methods part I) and extrapolated this to existing empirical data. The main goal was to assess the applicability of the previously adopted system identification approach to empirical data, in this case resting-state MEG time-series of Parkinson's disease patients. For this I used existing resting-state MEG data as selected and used in previous studies [2-3]. An overview of the described method is illustrated in Figure 2.
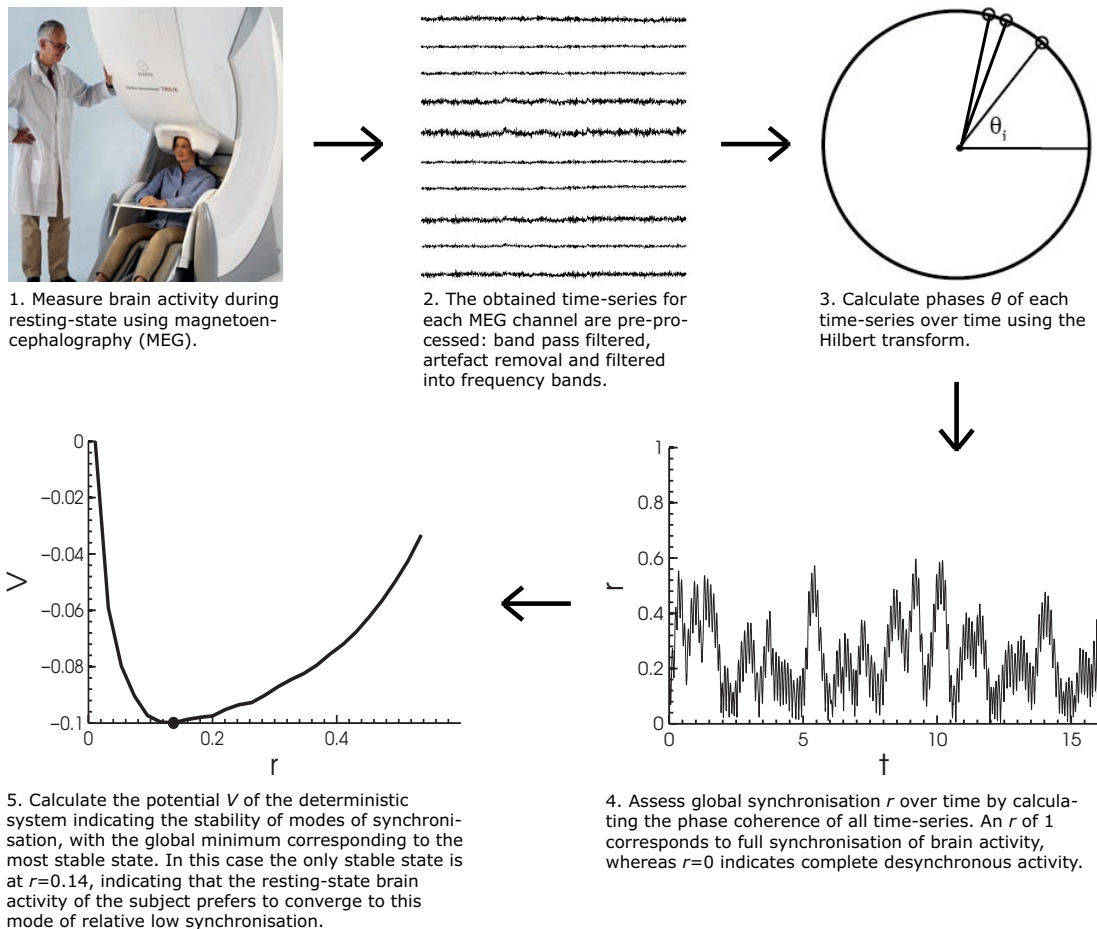
---

[2] The Matlab source code for Kramers-Moyal coefficient estimation is available from the authors on request.

A total of 70 Parkinson's disease (PD) patients along with 21 healthy controls have been selected for analysis and measured in a previous study by Stoffers and co-workers [2-3]. The PD patients were divided into four subgroups based on their disease duration, i.e. a group of newly diagnosed, untreated patients (N=18), a group of mild PD patients (N=19, disease duration of 3-5 years), a group of mild-moderate PD patients (N=16, disease duration 6-8 years) and a group of moderate PD patients (N=17, disease duration = 9-11 years). The latter three groups include 37 levodopa-treated PD patients. The self-declared healthy controls have been age-matched with the newly diagnosed, untreated patient group and consist of spouses of patients and healthy volunteers.

Disease duration was determined by the patients' subjective estimate of the time of occurrence of first motor symptoms, which has been shown to correlate well with both medical records and estimates from face-to-face interviews with a medical professional [53]. Furthermore, a number of subject characteristics were determined as described previously and in more detail by Stoffers et al. [3]. These measures include level of education using the International Standard Classification of Education [54] and premorbid intelligence using the National Adult Reading Test (NART) [55]. For the Parkinson patients a number of additional subject characteristics were determined. These include time of disease onset and disease rating sub scores using the Unified Parkinson's Disease Rating Scale motor scores (UPDRS-III) [56] and modified Hoehn and Yahr stages [57], both obtained by a training physician prior to MEG registration in the "practically defined OFF" state as defined by the CAPIT Committee [58].

1. Measure brain activity during resting-state using magnetoen-cephalography (MEG).

2. The obtained time-series for each MEG channel are pre-processed: band pass filtered, artefact removal and filtered into frequency bands.

3. Calculate phases θ of each time-series over time using the Hilbert transform.

5. Calculate the potential V of the deterministic system indicating the stability of modes of synchronisation, with the global minimum corresponding to the most stable state. In this case the only stable state is at $r=0.14$, indicating that the resting-state brain activity of the subject prefers to converge to this mode of relative low synchronisation.

4. Assess global synchronisation r over time by calculating the phase coherence of all time-series. An r of 1 corresponds to full synchronisation of brain activity, whereas $r=0$ indicates complete desynchronous activity.

Figure 2 | From MEG to synchronisation dynamics using a system identification approach.

MEG data acquisition and pre-processing

MEG data acquisition and pre-processing were largely performed as described previously [3]. Subjects were recorded using a 151-channel whole-head radial gradiometer MEG system (CTF Systems Inc., Port Coquitlam, BC, Canada) at the VU medical centre in Amsterdam. The recording band pass was set to 0.25-125 Hz with a sample rate of 312.5 Hz. Levodopa-treated patients were recorded in the "practically defined OFF" state. MEG of

all subjects was recorded in an eyes-closed resting-state condition. Of the 151 channels, a total of 12 channels were excluded due to technical problems of some sort, thus leaving a total of 139 channels per subject (see [59] for more information). For further analysis the MEG was converted into ASCII-files and imported into a commercial software package (MATLAB 7.14, The Mathworks Inc., Natick, MA, 2000). Subsequently a pre-processing procedure as described by Olde Dubbelink and co-workers [59] was applied, i.e. split up all subject registrations into epochs of 5000 samples (16s) and exclude all channels and epochs containing artefacts for further analysis. Artefacts that excluded epochs from selection were, e.g., muscle activity and eye movements affecting one or multiple channels. Note that pre-processing is necessary to guarantee stationarity of the data required by the system identification approach applied later.

Since I was mainly interested in validating whether the approach still holds for small sample-sizes of resting-state time-series and to explore its functional relevance as a diagnostic tool, I restricted the data set to only two subjects within each of the three defined subgroups (control, newly-diagnosed PD patients and moderate PD patients). Subject selection was based on gender (male), age and level of education.

Data analysis
Due to limited availability only four trials (consisting of 5000 samples or 16 s each) per subject were taken into account. For simplicity the study was limited to a single frequency band, i.e. the alpha1 (8-10 Hz) frequency band. The choice for the alpha1 band was based on the wide variety of results reported in this frequency range in studies on Parkinson's disease patients [2, 59-60]. Subject trial time-series were thus filtered with a second order Butterworth band pass filter in the alpha1 (8-10 Hz) frequency band. Note that due to this filtering, rapid changes in the time-series were excluded. This was not a problem since I was mainly interested in extracting the order parameter, i.e. the slowest dynamical variable in the system.

To obtain the phase of the MEG data the analytic signal $X_c(t)$ for each configuration c (i.e. different subject, trial and channel) was calculated by applying the Hilbert transform:

$$X_c(t) = x_c(t) + iw_c(t), \tag{6}$$

with $x_c(t)$ and $w_c(t)$ corresponding to the real and imaginary parts of the complex time-series $X_c(t)$, where the real part $x_c(t)$ was the original time-series and $c=\{$subject, trial, channel$\}$. Next the phase $\theta_c(t)$ of each original MEG signal space time-series was extracted using the analytic phase obtained from Eq. (6) such that

$$\theta_c(t) = \arctan\left(\frac{w_c(t)}{x_c(t)}\right). \tag{7}$$

Considering the source-space MEG time-series as a system of coupled oscillators allowed for a calculation of the phase coherence r using (3) for each subject and trial with N the number of MEG channels. Following the similar system identification approach as mentioned earlier to the system of coupled phase oscillators (see Methods part I) the drift coefficient $D^{(1)}$ was estimated and subsequently its potential was assessed (see Figure 2). Contrary to the earlier performed analysis, the diffusion coefficient $D^{(2)}$ was also estimated for all subjects. Due to the highly descriptive nature of the second part of this study no statistics measures were adopted.

Results part I

Preferential rewiring model

The number of hubs as quantified using node degree steadily increased with rewiring step S for all adopted hub measures (Figure 3). For the non-fixed threshold, i.e. $k_h > \langle k \rangle + \sigma$, the number dropped at $t \cong 60$ with sharply increasing variance. This drop was due to the definition of the hub threshold in combination with the discreteness of node degree: as the standard deviation of the distribution continued to increase from zero with S, the hub threshold rose concurrently. As the hub threshold reached a discrete node degree value, a large number of nodes became excluded and the hub number sharply dropped. For fixed hub thresholds ($k_h > 4,5,6$) the number of hubs increased throughout the full range of S. In the following results I adopted the fixed hub threshold $k_h > 5$ to quantify hubs and normalised this by the size of the network to find hubness H.
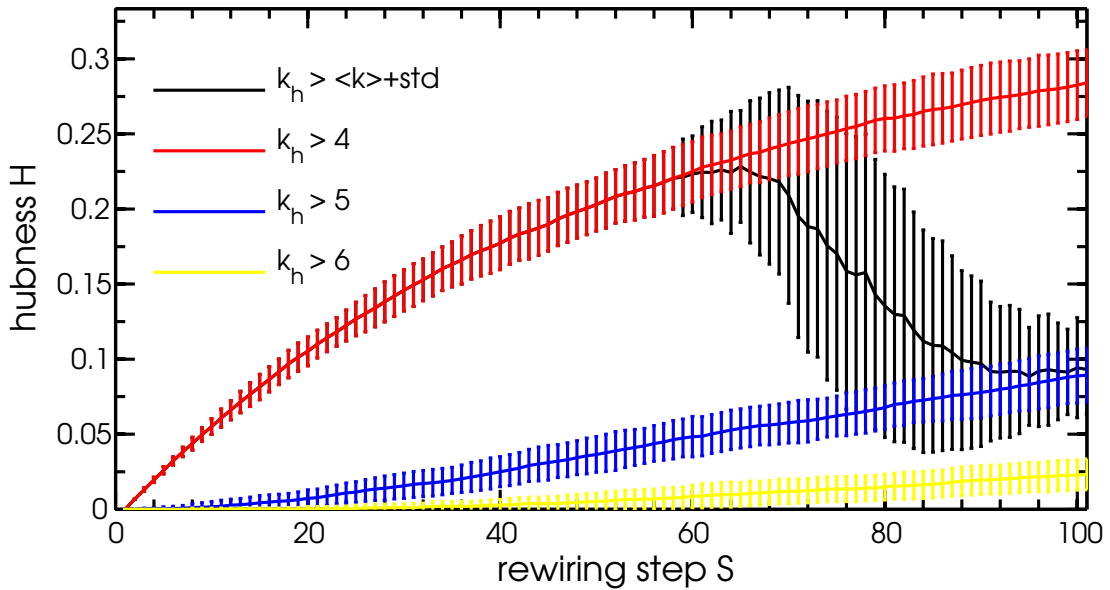
Figure 3 | The fraction of hubs in the total network, i.e. hubness H, as a function of rewiring step S. As the network was rewired with S the hubness increased for all four hub measures used. For all fixed measures ($k_h > 4, 5, 6$) hubness was seen to increase throughout the full range of S. The variable measure ($k_h > \langle k \rangle + \sigma$) was seen to transition from the $k_h > 4$ to the $k_h > 5$ threshold measure between $S = [60, 100]$. The transition occured due to an increasing node degree variance with S; this caused nodes previously quantified as a hub node to become excluded.
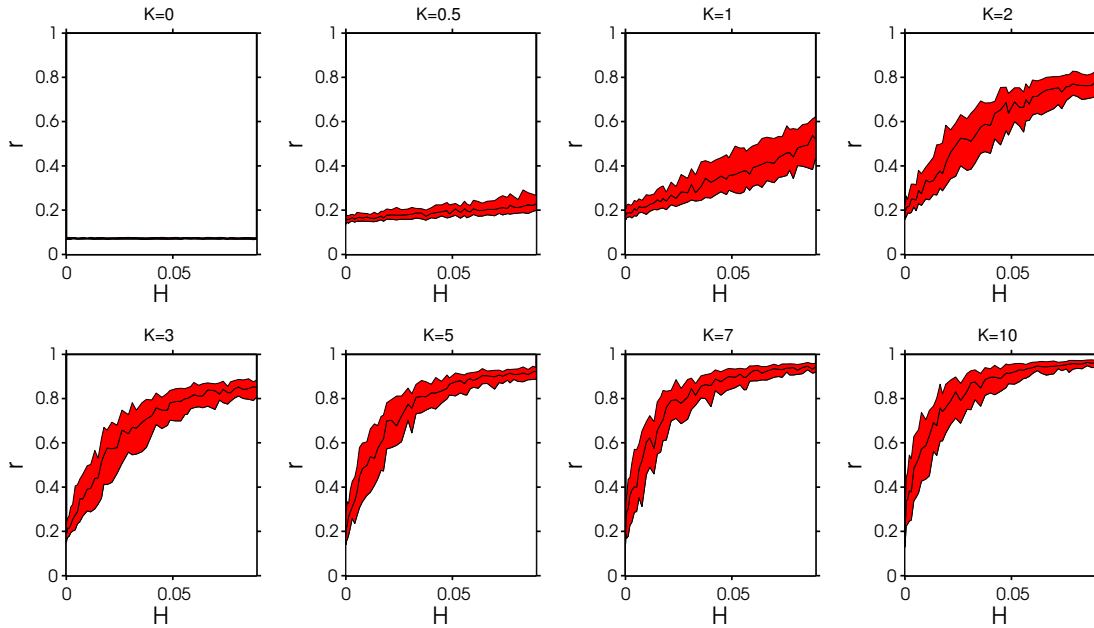
Global network synchronisation

Changes in global synchronisation r as a function of overall coupling strength K and hubness H are illustrated in Figure 4. First to notice is that global synchronisation of the network of coupled oscillators was, besides being dependent on global coupling as expected, also markedly influenced by H. Although network topology was seen to have little to no influence in the weakly coupled regime ($K \lesssim 2$), in the stronger coupled regime global synchronisation of the network of coupled phase oscillators was observed to increase as the number of hubs, i.e. hubness, increased. The same holds for network hubness: as the network was close to a regular topology
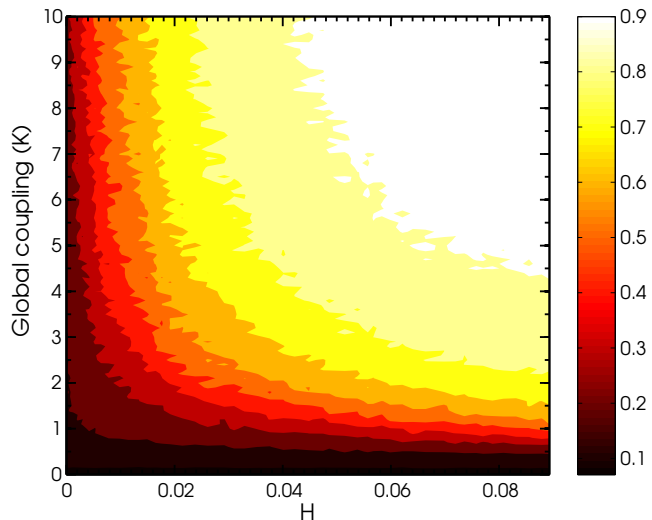
Figure 4 | Global network synchronisation r as a function of hubness H and global coupling K.

10

with corresponding low hubness ($H \approx 0$) global coupling had limited influence on network synchronisation. The largest changes in r were observed for $K = [0.5, 2]$ with high H and $H = [0, 0.02]$ with high K.
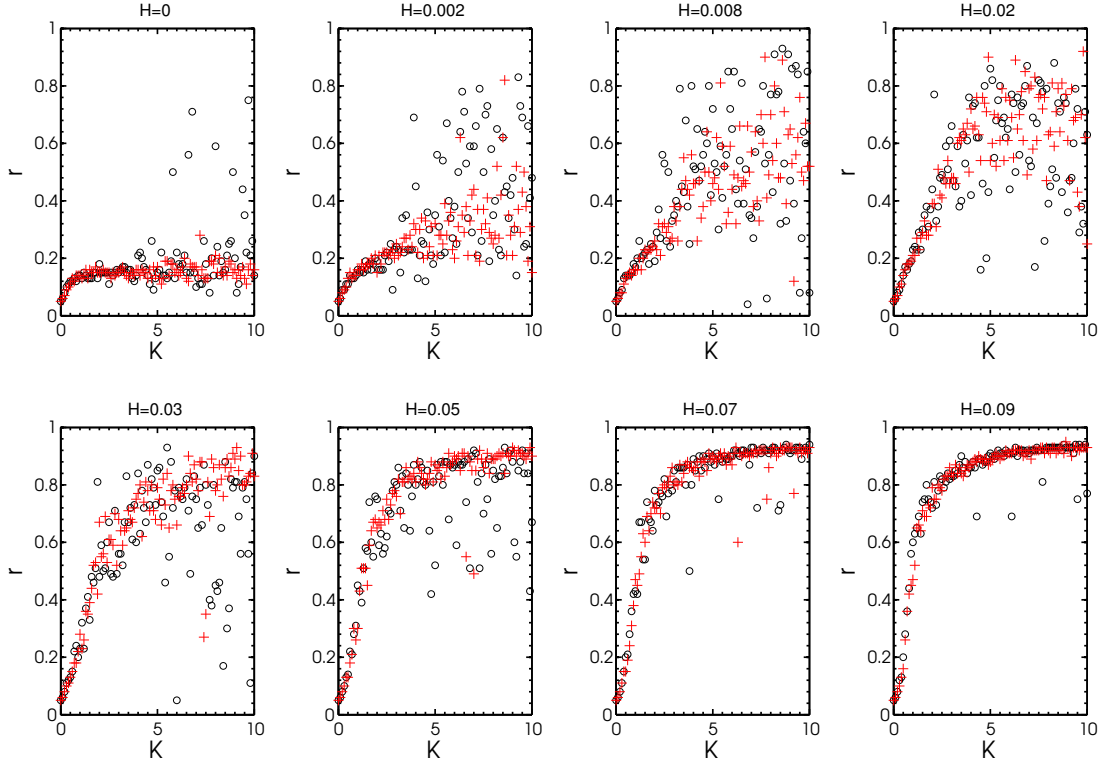

Figure 5 | Global synchronisation r as a function of H and K (different panels). Since the distribution of r was not normal the median is shown; the red areas represent the interquartile range. Global synchronisation of a network of coupled oscillators was seen to depend on both global coupling and hubness.

Interestingly, strong coupling and a high hubness were both required for maximal global network synchronisation. Failure to obtain maximal synchronisation at low hubness can be attributed to the high characteristic path length of the corresponding networks and thereby the inability for oscillators to interact successfully. A lack of central nodes thus seems to suppress the network to obtain full global synchronisation. A more detailed visualisation of global synchronisation including an estimation of variability is shown in Figure 5. In the strongly coupled ($K \rightarrow 10$) regime small increases in hubness had a large influence on network synchronisability. These results suggested that hubness had a great influence on whether a network was able to synchronise, where even deviations as small as a few rewired connections altered network synchronisability.

Synchronisation dynamics
To further investigate the system's deterministic dynamics, the first Kramers-Moyal coefficient, i.e. the drift coefficient $D^{(1)}$, was estimated. Global minima of the drift coefficient's potential, corresponding specifically to the root of the drift coefficient and the most stable state of the deterministic system in general, are shown in Figure 6. First thing to notice is that as hubness H increased with rewiring S, the global minima were found close to full synchronisation values, i.e. $r \rightarrow 1$, suggesting that global synchronisation occurred as the most stable state. At the regular ordered network ($H = 0$, top left panel in Figure 6) the deterministic system preferred an unordered state for all K values within the simulated range. As hubness increased and the network became less ordered, synchronising behaviour from low H on was observed in the strongly coupled regime. It was clear that changing the topology by preferential rewiring from a regular ordered network boosted the stability of the globally synchronised state. However, I observed a large transient regime where only partial synchronisation was attained and it was in this critical regime that a lot of locally stable states emerged and coexisted (Figure 7). This critical regime spanned approximately from the initial emergence of hubs ($H \approx 0.002$) until $H \approx 0.05$ in the semi-weak to strongly coupled regime ($K \approx [2,10]$). Note that the true critical regime could be spanning beyond $K = 10$ for some H.
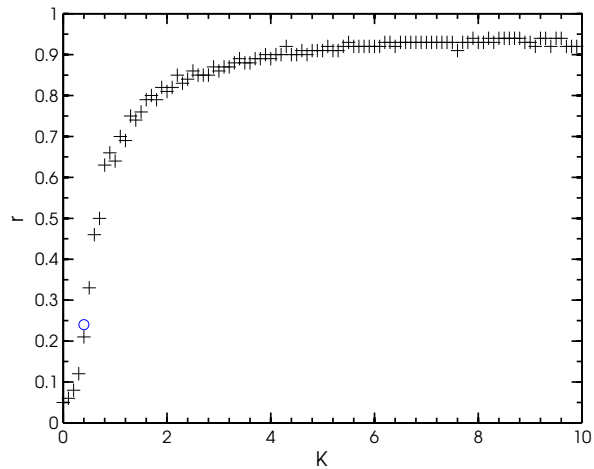
Figure 6 | Global minima of the potential of drift coefficient $D^{(1)}$. Values of r are plotted for both the noise-free model ($Q = 0$, black dot) and noise model ($Q = 0.1$, red plus) as a function of both K and H (different panels). Noise-induced synchronisation was observed as a reduced variance in r over K. The hubness H corresponded to an average number of hubs of respectively (from left to right, up to down): 0, 0.3, 1.2, 3, 7.5, 10.5 and 13.5.
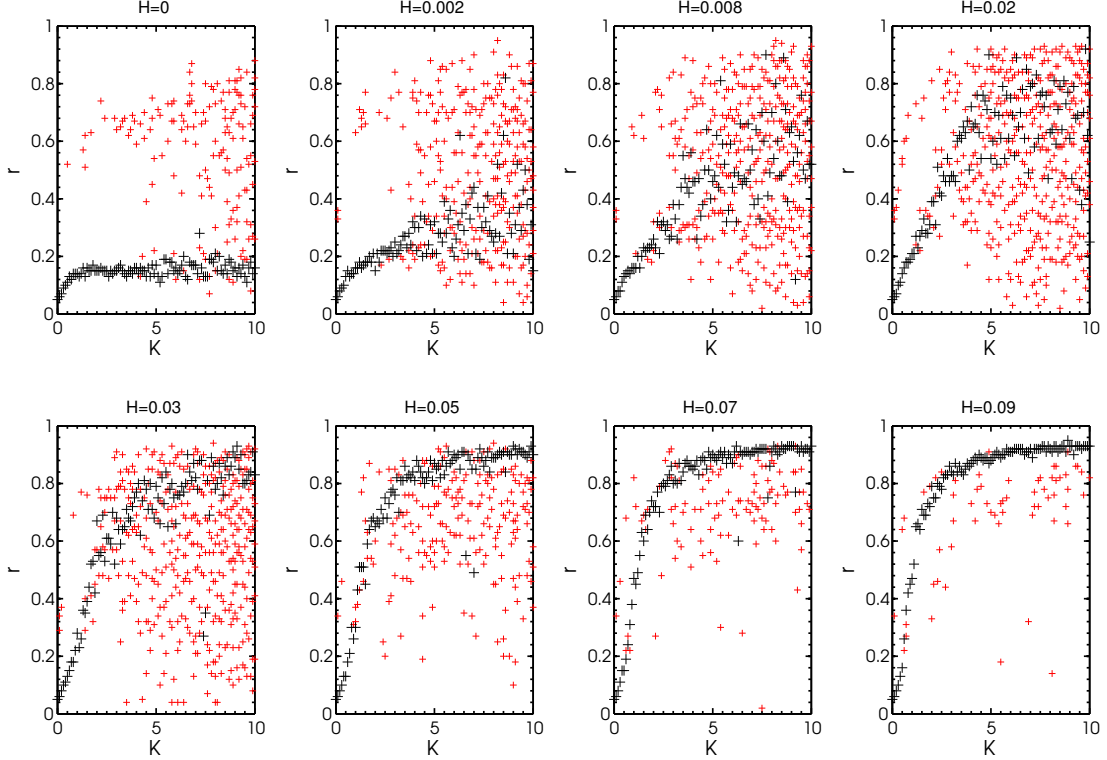
Figure 7 | Global (black) and local (red) minima of the potential of the drift coefficient for the noise-induced $Q = 0.1$ network topology. Values of r are plotted as a function of K and H (different panels). The occurrence of local minima increased with initial increases of H and decreased at higher H. The global minima corresponding to the most stable state of the system converged to full synchronisation for high H and K. The hubness H corresponded to an average number of hubs of respectively (from left to right, up to down): 0, 0.3, 1.2, 3, 7.5, 10.5 and 13.5.

12

In order to investigate the influence of noise on a system's ability to synchronise I induced a second model with stochastic force $Q = 0.1$. For the model which excluded noise ($Q = 0$) I observed a very long transient regime for S with respect to global network synchronisation. For the latter model I saw a noise-induced stabilisation occur (Figure 6, plus markers), i.e. the network was seen to reach a stable state of global synchronisation at a lower hubness value H with respect to the $Q = 0$ model and showed an overall reduced variation in r. The transient regime entailing partial synchronisation, however, was still present. A second observation seen in both models was the presence of multiple roots in the drift coefficient (Figure 7). Even for $Q = 0.1$ a lot of local minima were present throughout the whole spectrum of K and S. For high S the local minima were seen to diminish in number, a higher hubness thus seemed to have a stabilising effect on synchronisability. However, initial rewiring from the regular topology ($H \sim 0.002 - 0.02$) only increased the number of local minima and thereby the number of locally stable states of the system.
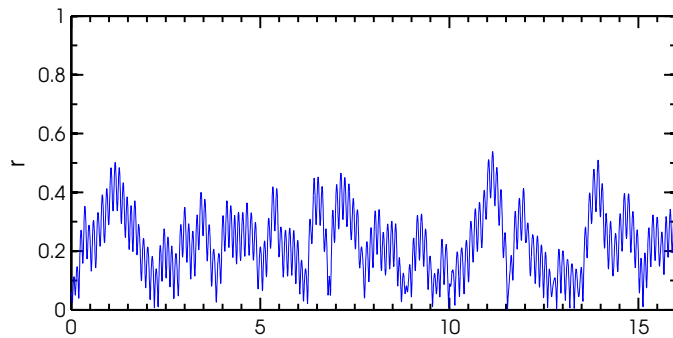

Figure 8 | Synchronisability of Erdös-Rényi networks with identical topological constraints. Global minima of the potential of the drift coefficient of r are shown as a function of K. Local minima (blue circles) were almost non-existing over the whole range of K.

As a reference I investigated random networks with the same topological constraints, results are shown in Figure 8 The random network clearly synchronised fully even for low K due to its low characteristic path length. More interestingly, the random network showed (almost) no local minima pointing out the fact that the only stable state of the random network was the globally synchronised. According to the hub threshold adopted earlier these networks have 30.5 ± 3.2 hubs on average.

Results part II

*Applicability of a system identification approach to empirical resting-state data*
I assessed the applicability of the previously shown system identification approach to empirical data, in this case resting-state MEG time-series of Parkinson's disease patients. Phase divergence r over time of a typical trial in the alpha1 band is shown in Figure 9. As can be observed, r was seen to increase and decrease over time within certain values up to $r \sim 0.5$ indicating local and/or global

Figure 9 | Phase divergence r over time as calculated over all MEG channels of resting-state time series. The value of r, representing global synchronisation, is typically seen to increase and decrease over time. In this case the phase divergence of subject 1, trial 1 in the alpha1 band is depicted.

synchronisation and desynchronisation patterns of the different brain network regions over time during resting-state.

Although limited sample sizes of time-series within trials constrained the quality of the Kramers-Moyal coefficient estimation, I was able to determine the drift coefficient (Figure 10, left panels) and its potential (Figure 10, right panels). Unlike the drift coefficients obtained in the simulated networks previously, the drift coefficient of the resting-state MEG time series showed only a single root for each subject, with a corresponding single minimum found in its potential. A potential of this form could be described by an even polynomial of higher order, i.e. a fourth order or higher. Interestingly, the potential of the drift coefficient showed marked asymmetric behaviour over r for all subjects. Visual inspection gave no indication of differences in global minima of either size or location between subject groups. In other words: the deterministic brain network during resting-

state seemed to prefer a similar stable state of global synchronisation across the different subject groups.
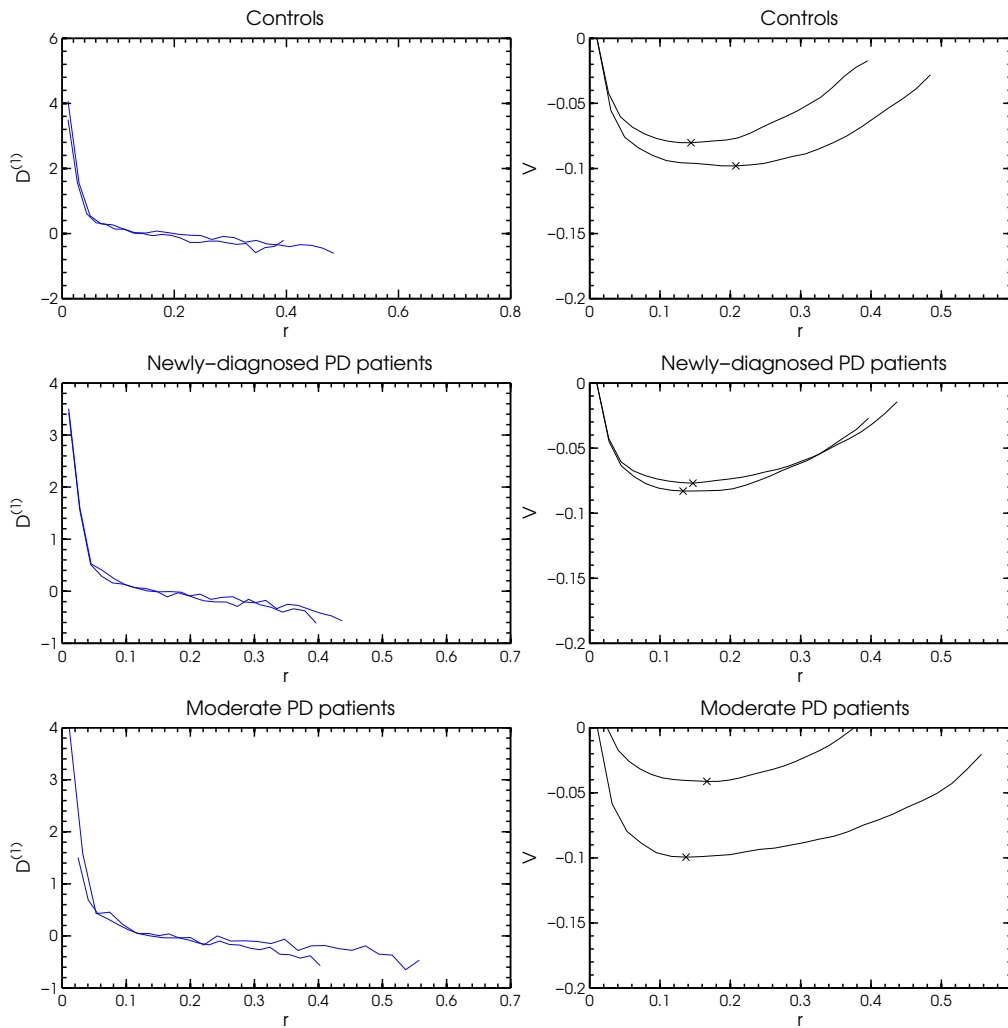
Figure 10 | Drift coefficient $D^{(1)}$ and its potential V over r for the different subject groups. The drift coefficient shows a single root for all subjects corresponding to a single stable state (attractor) of the network, in this case the resting-state brain. The root of $D^{(1)}$ is further investigated by visualising its potential showing a single minimum for all subjects.

The diffusion coefficient $D^{(2)}$, depicting the stochastic components of the resting-state brain, is shown in Figure 11. The diffusion coefficient is found to be globally constant over the range of r for most subjects. Locally $D^{(2)}$ is seen to have some large increases, suggesting the presence of synchronisation-dependent noise. However, since the amount of samples is so small, no conclusive results can be drawn from these findings.
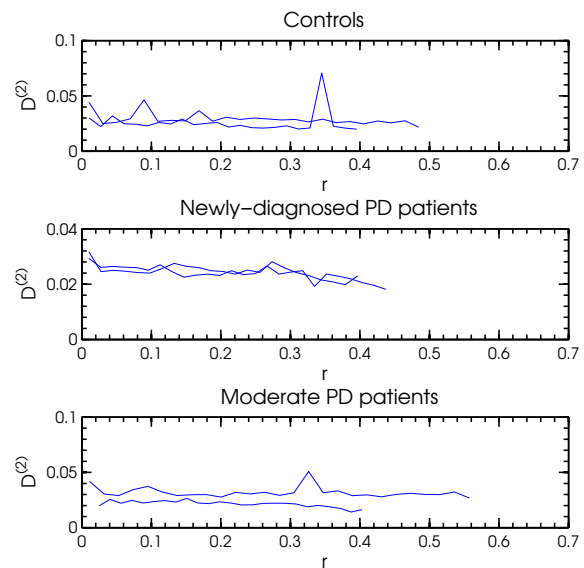
Figure 11 | Diffusion coefficient $D^{(2)}$ over r for the different subject groups. $D^{(2)}$ is constant over the whole range except for local increases observed in some subjects.

14

Discussion

General conclusions
In this study I adopted a preferential rewiring model which showed an increase in hubness. An increase or decrease in hubness H has profound effects on global synchronisation of sparsely coupled networks as found in the human brain. Also, the presence of hubs, together with sufficient coupling, is a primary prerequisite to obtain global synchronisation as a stable state. More interestingly, a low-to-medium H induces an emergence of locally stable states of partial synchronisation, which could not be explained by an increase in randomness. Lastly I adopted the same approach to resting-state MEG data of PD patients to test its applicability. The approach was able to show minima in the potential of the drift coefficient for all subjects. Although this approach did not highlight any differences between patient groups, the method seems feasible as an unbiased future diagnostic tool in Parkinson's disease and other neurodegenerative diseases affecting cortical synchronisation, however, more research is needed. The following paragraphs hold an in-depth discussion on these results.

Preferential rewiring model
I adopted a model based on the non-growing scale-free network model proposed by Xie and co-workers [27] to study the effect of hubs on synchronisability of sparse networks. The rewiring procedure as proposed indeed induces hubs as quantified using the common definition based on a fixed node degree [45]; the chosen measure to quantify hubs however was not trivial. This problem arises from the fact that a hub node is poorly defined in literature and no general consensus to its measure exists. In the graph theory hubs are defined as well-connected nodes [45]. In brain networks additional criteria arise defining hub nodes as high-degree nodes central to the network (i.e. high degree centrality, low characteristic path length, low clustering coefficient and high aggregation of characteristic motifs) [61]. However, in studies on brain networks the most commonly used hub measures are solely based on one characteristic, such as node degree [62-63] or path length [64] whereas only a small number of studies consider multiple measures [65-66]. The current results defining hubs using a variable node degree ($k_h > \langle k \rangle + \sigma$) in an unweighted network clearly shows the bias of this measure when comparing networks with a changing distribution or varying standard deviation. To avoid this bias a fixed hub threshold based on node degree can be adopted. This, on the other hand, does not necessarily guarantee an increase in overall hub quality: as more nodes are qualified as hubs, the centrality characteristics of these nodes with respect to the other network nodes might decrease. As a critical note, I therefore would like to stress the importance of selecting a suitable hub measure, considering its applicability on the network and taking notion of its implications.

The previously described problem with hub definition also leads to the issue of defining networks with a changing hubness in a controlled setting. The adopted model includes preferential rewiring to obtain hubs and seems successful in achieving so. However, the effects found could still be an effect of rewiring rather than an increase in the number of hubs. To test for this one could argue to compare the modelled networks with for instance Watts and Strogatz (WS) random rewiring networks [38] with intermediate values for rewiring probability p or random networks with $p = 1$ (i.e., Erdös-Rényi networks [37]), but these networks would still possess high degree nodes (i.e., hubs) [40]. As a solution one may use a rewiring WS network for comparison that does not allow for the emergence of hubs, e.g. by constraining rewiring of connections to nodes with a degree close to the hub threshold. The practical implementation of such a network could prove hard for small networks and I would like to stress here that the emergence of hubs in such a network is still only dependent on the selected hub threshold. A less solid solution used in this study is the comparison of my modelled networks with those of Erdös-Rényi networks after rewiring has taken place. A direct consequence of rewiring on a network is an increase of randomness; hence this allows us to assess effects of randomness on synchronisability as imposed by these networks.

Network synchronisation
An increase in the number of hubs positively affects the ability for a phase oscillator network to synchronise. In fact, a high hubness H seems to be a primary requisite for obtaining (semi-) full global synchronisation. Furthermore I observed a broad transient interval for H in which global synchronisation is not attained and a lot of partially synchronised states coexist as stable and unstable network states. In particular the

emergence of multiple local minima in the potential of $D^{(1)}$, corresponding to locally stable states of the network of a, in most cases, partially synchronised state, indicates the existence of a hub-induced multistability and possibly an area of self-organised criticality [67]. Systems possessing such self-organised criticality typically show a large functional repertoire. Recently, self-organised criticality has been hypothesised to appear as an attractive mode for normal brain functioning [68-70] since it optimises information processing [71]. Combining this knowledge with my findings suggests that hubness could be key to self-criticality in sparsely coupled networks including highly complex networks such as the brain cortex. A small deviation in this hubness could thus cause a loss of criticality and thereby a decrease in functional repertoire. Extrapolating this, I hypothesise that a deviation in hubness in the human brain network might even be able to explain a loss of criticality and functional diversity as for instance observed in cortical brain activity of epilepsy patients [72].

Although a transient regime for H is clearly present, it is not clear how and where this transient regime spans exactly or if any critical hubness value H_c is present as has been widely shown for global coupling in Kuramoto networks [14]. It is expected that the rather large size of the observed transient can mainly be attributed to the considerable between-repetition variability in hubness combined with limitations within the estimation of the Kramers-Moyal coefficients (i.e. 'the more samples the smaller the deviation', [73]). A larger number of repetitions in the order of at least 10^4 is desired to further investigate the exact location and form of this phase transition. Unfortunately due to lack of computational power and time constraints, it is beyond the scope of this study to examine this in more detail.

As a reference network I examined Erdös-Rényi networks [37] with similar topological constraints on the following question: to what extend can the effects of H on synchronisability be accounted for by the increasing randomness of the evolving network and what is indeed induced by the increase in hubness? A general conclusion here is that the increase of randomness in the evolving network indeed seems to boost synchronisability. Therefore, the observed increased (stability of) global synchronisability with H can very well be attributed to an increase in randomness of the network. However it does not explain the emergence of (un)stable states of partial synchronisation for low-to-medium H nor does it explain how and where the transient (i.e. phase transition) occurs. I therefore consider these latter results a mere effect of hubness.

The emergence of coexisting unstable states as a function of hubness needs further investigation. I would like to propose that the increase in functional repertoire corresponding to an increase in the number of coexisting (locally) stable states could be caused by different competing patches of hubs. To test this hypothesis I suggest an examination of the local synchronisation patterns within the evoluting topologies. As hubs emerge due to preferential rewiring I expect these nodes to form clusters with their own preferred oscillating frequency resulting in competing behaviour of different patches of hubs, thereby creating an increase in functional states. To test this, local synchronisation [74] can be calculated to see whether these hub communities exhibit full local synchronisation in the critical transient regime. Additionally modularity could point out to what extent different modules are present as a function of rewiring or hubness. These results are particularly interesting in the scope of human brain networks since the brain is known to have several resting state networks that are alternatingly activated in time [75]. Further investigating this behaviour in a controlled setting could be beneficial to a better understanding of the brain network.

Applicability of a system identification approach to empirical resting-state data
A system identification approach based on the estimation of Kramers-Moyal coefficients was shown to successfully identify stable synchronisation modes and stochastic components of resting-state MEG time-series of Parkinson's disease patients. However, the observed potential showed only one minimum for each subject and size and location of this global extremum did not differ in size or location between patient groups. Extrapolating findings found in the first part of this study suggested the presence of local minima in the potential for the empirical data. A two-sided explanation for these unexpected results can be proposed, i.e.: data limitations and an assumption bias. The first of these entails the straightforward explanation, i.e. the limited number of data samples used in combination with the high correspondence of the quality of the approach on the number of samples available (discussed in further detail in next paragraphs). However, testing the approach on a comparable sample size of data from the first part ruled out this possibility: the system identification procedure was still able to reveal local minima. On the other hand,

the limited sample size did hamper the resolution of the estimation of the drift coefficient and thereby its potential. Minima close to the global minimum could thereby have been ending up in the same bin as the global minimum and thus filtered out as a local extremum. A higher sample number, as also discussed in later paragraphs, could thus offer a solution to reveal possible local minima close to the global minimum. However, I would like to stress that this only offers a minor explanation to the observed single minimum observed in the empirical data.

As a second, more solid explanation I would like to propose an assumption bias, i.e. that of the sparsity of the network. In the first part of this study, i.e. the simulations, function emerged on top of an imposed structure. The sparsity of the simulated structures was thought to reflect the sparsity in true structural brain networks of 3% as reported by Hagmann and co-workers [41]. In the second part of this study resting-state MEG time-series were assessed. Resting-state functional connectivity which, although is thought to reflect the underlying structural network [91], does not necessarily imply that functional connections reflect structure per se [92] In other words: sparsity of structural and functional brain network might differ to a large extent. In fact, the observed single potential for all subjects showed more similarities to those observed for all-to-all coupled networks of stochastic phase oscillators with low global coupling [93]. This suggests that the functional resting-state network as studied in the second part might not have been as sparse as assumed and did not reflect the simulated sparse networks. To check for this one could assess and compare the functional connectivity of both the simulated and empirical data. However, due to time limitations this was not carried out.

Since Parkinson's disease is characterised by stage-dependent disturbances in network synchronisability [60] the results suggest that an application of this method might serve as an unbiased qualitative diagnostic tool to classify PD patients in addition to the rather quantitative and occasionally subjective measures used nowadays (i.e. disease duration, UPDRS scale [56], Hoehn and Yahr staging [76] and/or LEDD) some of which neglecting variability in disease progression between patients [77]. Alternative possible applications of the presented method, including classifying other (disconnective) neurodegenerative diseases that have been reported to show topological changes in the functional brain network (e.g. Alzheimer's disease [8, 78], schizophrenia [79-80] and multiple sclerosis [81]) require further exploration. Furthermore, it could give insight into these pathology-induced topological changes in the functional and possibly structural brain network. It could thus serve as a predictive tool; assessing disease severity and predicting prognosis of pathology.

A minor finding in this study includes the non-parametric behaviour of the potentials of $D^{(1)}$ found for the analysis of the resting-state MEG time-series in the alpha1 band. Although this study was not aimed to find any conclusive results, the findings are conflicting with those of Hindriks and co-workers, who suggest that resting-state MEG activity in the alpha1 band can be modelled as weakly coupled self-sustaining linear oscillators [82]. However, since the number of samples and the type of subjects differs greatly between studies, the earlier findings of Hindriks do not necessarily contradict the present findings although additional analyses could.

Two main limitations for the application of the proposed method on Parkinson's disease data as performed in this study arose: the number of samples and the use of MEG. The first limitation proved to be very important since the quality of the system identification procedure as applied in this study is known to be highly dependent on the amount of data samples [73]. In this study, however, the amount of samples was confined which restricted the estimation of probability transitions needed to calculate the Kramers-Moyal coefficients thereby hampering the quality of the extracted dynamics [49]. For a more thorough estimation of the coefficients and thus the network dynamics, an increase in the number of data samples are highly recommended either through more trials or longer trial length. Note that increasing sample size by an increased sample frequency is not a solid solution to this problem since this only offers a more detailed view on a system's dynamics rather than increasing the dynamical scope covered by the data.

The second limitation involves the stationarity of the process under study. One has to keep in mind here that throughout the procedure I assume the dynamical process under study to be stationary, i.e. it is a Markov process. To test for this, the experimental data should obey the Chapman-Kolmogorov equation as presented in the Methods; however, this was beyond the scope of this study. Also, when measuring brain processes, especially during resting-state, at longer time scales this criterion may no longer be valid. I would like to stress here that the application of a system identification method of the dynamical brain network during resting-state critically depends on the trade-off between a large

17

enough number of samples to assure quality of the estimation on the one hand and limiting the number of samples such that stationarity is retained on the other hand. There are a number of possibilities to work around this trade-off that I would like to briefly propose here: it would be possible to increase the quality of the probability transitions by limiting the degrees of freedom by parameterising these expected probability transitions. On the other hand, extending the experimental recording time (e.g. by repetitive recording [73] to obtain more samples could be used to greatly enhance the quality of the procedure. However, this will induce additional time scales to be incorporated in the experimental design and subsequent analysis that may require a change in the experimental paradigm. A more in-depth study into the stationarity constraint and the discussed trade-off was beyond the scope of this study. However, since both stationarity and the number of samples are of great importance of the quality of Kramers-Moyal coefficient estimation and thereby the proposed system identification approach; hence, this could certainly be a subject of further study.

The second limitation one should consider is the use of MEG for the assessment of Parkinson's disease patients. Since early stage Parkinson's disease is considered a pathology of the subcortical regions [83-85] the need for an analytical approach assessing the cortical regions using MEG seems small. However, MEG abnormalities have been reported to be present from newly-diagnosed Parkinson's disease patients onwards [2, 86] suggesting that cortical degeneration is already present at onset of pathology. Therefore, I do not consider this a limitation for the approach. Another limitation involving the use of MEG is volume conduction. This bias is especially likely to influence source data (raw MEG data) as used in this study: that is, MEG sensors are likely to pick up activity originating from the same source, possibly causing a positive bias in the calculation of the global synchronisation r for subjects. However, since the proposed approach focuses on detecting between-subject differences in r rather than within-subject differences volume conduction is not considered to be an issue.

A recommendation for the application of the proposed approach would be to employ MEG data involving motor or attention tasks instead of resting-state MEG, thereby inducing a higher level of global synchronisation. The presented results showed that resting-state MEG data entails the partially synchronised regime [0.1,0.5] where motor or attentional tasks induce event-related synchronisation and desynchronisation [87] with reported differences in synchronisability between Parkinson's disease patients and healthy controls [88-90]. The system identification approach could prove to identify these differences between subjects based on MEG measurements during tasks, however, more research is needed.

To conclude, I was able to successfully apply a system identification approach based on the estimation of Kramers-Moyal coefficients on resting-state MEG data of Parkinson's disease patients. Taking into account the suggested limitations and recommendations, the proposed method could provide medical assessors with an unbiased tool to classify Parkinson's disease patients and offers possibilities for the extrapolation to other neurodegenerative diseases known to affect cortical synchronisability. Additionally, it could offer a solid approach to gain further insight into hubness of brain processes known to function in the self-organised critical regime and could prove as a prognostic tool in NDDs to predict disease progression. However, further research is needed.

Appendix A – Network Validation

Complex network measures were used to evaluate the preferential rewiring procedure and the corresponding developed network topology. These measures are: clustering coefficient C, characteristic path length, efficiency and centrality. A total of hundred repetitions were used to calculate each of these measures as a function of rewiring step S. Results were compared to Erdös-Rényi random networks with similar topological constraints (Figure A1).
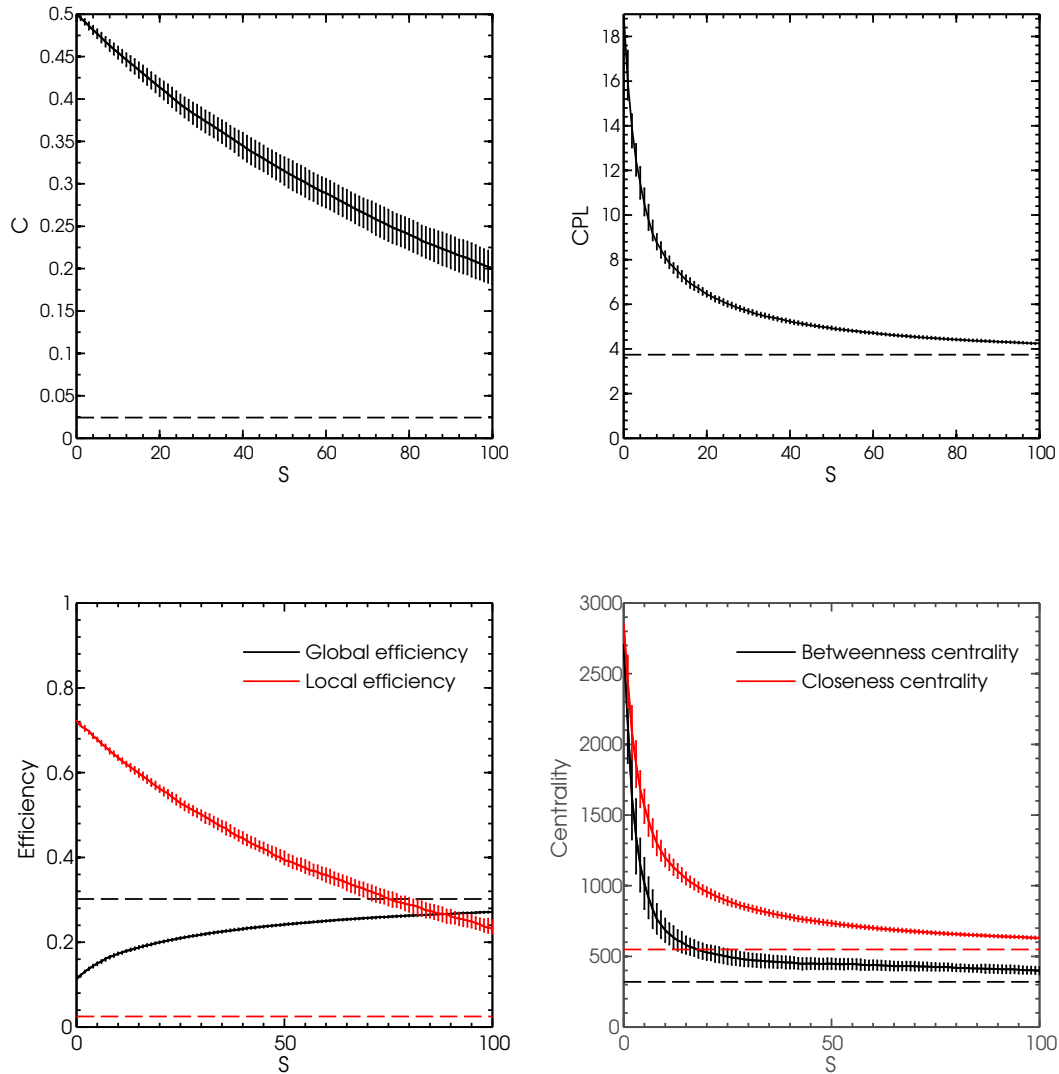

Figure A1 | Complex network measures as calculated for the preferential rewiring networks (solid lines) as a function of rewiring S and random networks (dotted lines). Most measures calculated for the preferential rewiring network converge to random network values at $S = 100$ except for the clustering coefficient and local efficiency.

First thing to notice is that all complex network measures converge to values expected in random graphs over S. Interestingly, although converging, both clustering coefficient (top left panel, Figure A1) and local efficiency (bottom left panel, Figure A1) still exhibit values not consistent with those expected for random graphs. The high clustering coefficient with a low characteristic path length qualifies the evolving network as small-world [38]. Typical features of such a network include enhanced synchronisability and signal propagation.

The probably most profound characteristic of a network topology entails the degree distribution. If the degree distribution of a network follows a power law, regardless of any other structure, it is said to be scale-free, i.e.

$$P(k) \sim k^{-\alpha}.$$

These networks lack a characteristic degree or scale and typically have an exponent $2 < \alpha < 3$. A classical method of inducing a hub-rich scale-free topology has been proposed by Barabasi and co-workers [25], although this does include increasing the node amount. Here, I chose a different methodology proposed by Xie and co-workers [27] adopting a non-growing network as to better approach empirical data (i.e. current knowledge of the human brain as a network does not agree with increases in brain regions or neurons) and exclude influences of N or k on any (network) measures. In Figure A2 is illustrated how the degree distribution flattens during rewiring, with a general increase in lower degree nodes suggesting a downward switch in node modus if rewiring would be elongated. Interestingly, I also observe a small but profound increase in relatively high degree nodes, i.e., hubs as rewiring step increases.
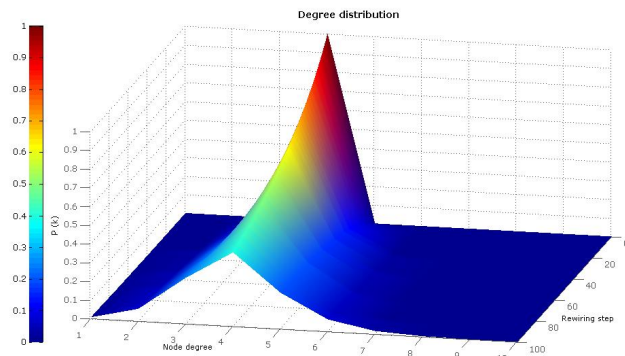
Figure A2 | Degree distribution as function of rewiring step S.

Acknowledgements

I would briefly like to thank some people who have helped me through the journey leading to the completion of my research master thesis. Firstly I would like to thank my supervisor Andreas for his serene guidance into and sincere help on interesting but very complex topics. Every time I thought it could not possibly get any more complicated, it did! Secondly I want to thank my family and friends for their unconditional support. A special thanks goes out to the following for reading through this dense work of complex sentences and/or providing me with helpful feedback along the way: my parents, Lee McFadden, Bernadette van Wijk, Eva Coopmans, Nico Jansen, Hanna van Lee, Marije Filius and Nathalie van Oomen.

References

1. Stam, C., *Use of magnetoencephalography (MEG) to study functional brain networks in neurodegenerative disorders.* Journal of the Neurological Sciences, 2010. **289**: p. 128-134.
2. Stoffers, D., et al., *Increased cortico-cortical functional connectivity in early-stage Parkinson's disease: An MEG study.* NeuroImage, 2008. **41**: p. 212-222.
3. Stoffers, D., et al., *Slowing of oscillatory brain activity is a stable characteristic of Parkinson's disease without dementia.* Brain, 2007. **130**: p. 1847-1860.
4. Wu, T., et al., *Changes of functional connectivity of the motor network in the resting state in Parkinson's disease.* Neuroscience Letters, 2009. **460**: p. 6-10.
5. Cronin-Golomb, A., *Parkinson's Disease as a Disconnection Syndrome.* Neuropsychol Rev., 2010. **20**(2): p. 191-208.
6. Greicius, M., et al., *Default-mode network activity distinguishes Alzheimer's disease from healthy aging: Evidence from functional MRI.* PNAS, 2004. **101**(13): p. 4637-4642.
7. Stam, C., et al., *Small-World Networks and Functional Connectivity in Alzheimer's Disease.* Cerebral Cortex, 2007. **17**: p. 92.
8. Haan, W.d., et al., *Disruption of functional brain networks in Alzheimer's disease: what can we learn from graph spectral analysis of resting-state MEG?* Brain Connect., 2012. **2**(2): p. 45-55.
9. Haan, W.d., et al., *Disrupted modular brain dynamics reflect cognitive dysfunction in Alzheimer's disease.* NeuroImage, 2012. **59**: p. 3085-3093.
10. Geschwind, N., *Disconnexion Syndromes in Animals and Man.* Brain, 1965. **237**.
11. Delbeuck, X., M.v.d. Linden, and F. Collette, *Alzheimer's Disease as a Disconnection Syndrome?* Neuropsychol Rev., 2003. **13**(2): p. 79-92.
12. Morgan, R. and I. Soltesz, *Nonrandom connectiviy of the epileptic dentate gyrus predicts a major role for neuronal hubs in seizures.* PNAS, 2008. **105**(17): p. 6179-6184.
13. Zhang, Z., et al., *Altered functional-structural couplilng of large-scale brain networks in idiopathic generalized epilepsy.* Brain, 2011. **134**: p. 2912-2928.
14. Kuramoto, Y., *Chemical Oscillators, Waves and Turbulence.* 1984, Berlin: Springer.
15. Acebrón, J., *The Kuramoto model: A simple paradigm for synchronization phenomena.* Reviews of Modern Physics, 2005. **77**(1): p. 137-185.
16. Brede, M., *Synchrony-optimized networks of non-identical Kuramoto oscillators.* Phys Lett A, 2007. **372**: p. 2618-2622.
17. Oh, E., et al., *Modular synchronization in complex networks.* Phys Rev E, 2005. **72**.
18. Matías, M. and J. Guémez, *Transient Periodic Rotating Waves and Fast Propagation of Synchronization in Linear Arrays of Chaotic Systems.* Phys Rev Lett., 1998. **81**(19): p. 4124-4127.
19. Pecora, L. and T. Carroll, *Master Stability Functions for Synchronized Coupled Systems.* Phys Rev Lett., 1998. **80**(10): p. 2109-2112.
20. Barahona, M. and L. Pecora, *Synchronization in Small-World Systems.* Phys Rev Lett., 2002. **89**(5).
21. Brede, M., *Synchronization on directed small worlds: feed forward loops and cycles.* Europhys Lett, 2008.
22. Hong, H., et al., *Factors that predict better synchronizability on complex networks.* Phys Rev E, 2004. **69**.
23. Moreno, Y. and A. Pacheco, *Synchronization of Kuramoto Oscillators in Scale-Free Networks.* Europhys Lett, 2004. **68**.
24. Wang, W., et al., *Onset of synchronization in weighted scale-free networks.* Chaos, 2009. **19**.
25. Barabasi, A.-L. and R. Albert, *Emergence of Scaling in Random Networks.* Science, 1999. **286**: p. 509.
26. Park, K. and Y. Lai, *Self-organized scale-free networks.* Phys Rev E, 2005. **72**.
27. Xie, Y., T. Zhou, and B. Wang, *Scale-free networks without growth.* Physica A, 2008. **387**: p. 1638-1699.
28. Evans, T., *Exact Solutions for Network Rewiring Models.* Eur. Phys. J. B, 2007. **56**: p. 65-69.
29. Friedrich, R. and J. Peinke, *Description of a Turbulent Cascade by a Fokker-Planck Equation.* Phys Rev Lett., 1997. **78**(5): p. 863-866.
30. Cohen, R. and S. Havlin, *Scale-Free Networks Are Ultrasmall.* Phys Rev Lett., 2003. **90**(5).
31. Colizza, V., et al., *Detecting rich-club ordering in complex networks.* Nature, 2006. **2**: p. 110-116.
32. Pereira, T., *Hub synchronization in Scale-Free Networks.* Phys Rev E, 2010. **82**.
33. Koch, C. and G. Laurent, *Complexity and the Nervous System.* Science, 1999. **284**(5411): p. 96-98.
34. Eguiluz, V., et al., *Scale-free brain functional networks.* Phys Rev Lett., 2005. **94**(1).
35. Heuvel, M.v.d., et al., *Small-world and scale-free organization of voxel-based resting-state functional connectivity in the human brain.* Neuroimage, 2008. **43**: p. 528.
36. Chialvo, D., *Critical brain networks.* Physica A, 2004. **340**(4): p. 756-765.
37. Erdos, P. and A. Renyi, *On the evolution of random graphs.* Publ Math Inst Hung Acad Sci, 1960. **5**: p. 17.
38. Watts, D. and S. Strogatz, *Collective dynamics of 'small-world' networks.* Nature, 1998. **393**: p. 440.
39. Ou, R. and J. Yang, *On structural properties of scale-free networks with finite size.* Physica A, 2012. **391**: p. 887-894.
40. Wijk, B.v., C. Stam, and A. Daffertshofer, *Comparing Brain Networks of Different Size and Connectivity Density Using Graph Theory.* PloS ONE, 2010. **5**(10).
41. Hagmann, P., et al., *Mapping the Structural Core of Human Cerebral Cortex.* PLoS Biol, 2008. **6**(7): p. 1479-1493.
42. Schmidt, H. and M. Jirstrand, *Systems Biology Toolbox for MATLAB: a computational platform for research in systems biology.* Bioinformatics, 2006. **22**(4): p. 514-515.
43. Scheinerman, E., *Matgraph Toolbox.* 2008. p. A Matlab Toolbox for Graph Theory.
44. Rubinov, M. and O. Sporns, *Complex network measures of brain connectivity: Uses and interpretations.* NeuroImage, 2010. **52**: p. 1059-1069.
45. Newman, M., in *Networks: An Introduction.* 2010. p. p. 245.
46. Newman, M., *Networks: An Introduction.* 2010.
47. Peinke, R.F.J., *Description of a Turbulent Cascade by a Fokker-Planck Equation.* Physical Rev Lett, 1997. **78**(5): p. 863-866.

48. Daffertshofer, A., *Benefits and Pitfalls in Analyzing Noise in Dynamical Systems - On Stochastic Differential Equations and System Identificiation*, in *Nonlinear Dynamics in Human Behavior*, R.H.V. Jirsa, Editor. 2010, Springer-Verlag: Berlin. p. 35-68.
49. Mourik, A.v. and A. Daffertshofer, *Deterministic and stochastic features of rhythmic human movement.* Biol Cybern, 2006. **94**: p. 233-244.
50. Friedrich, R., J. Peinke, and C. Renner, *How to Quantify Deterministic and Random Influences on the Statistics of the Foreign Exchange Market.* Phys Rev Lett., 2000. **84**(22): p. 5224-5227.
51. Mourik, A.v., A. Daffertshofer, and P. Beek, *Extracting Global and Local Dynamics From the Stochastics of Rhythmic Forearm Movements.* Journal of Motor Behavior, 2008. **40**(3): p. 214-231.
52. Pawula, R., *Approximation of the Linear Boltzmann Equation by the Fokker-Planck Equation.* Phys Rev, 1967. **162**(1): p. 186-188.
53. Reider, C., et al., *Reliability of reported age at onset for Parkinson's disease.* Mov. Dis., 2003. **18**(3): p. 275-279.
54. UNESCO, *International Standard Classification of Education 1997*, U.I.o. Statistics, Editor. 2003: Montreal.
55. Nelson, H. and A. O'Connell, *Dementia: the estimation of premorbid intelligence levels using the New Adult Reading Test.* Cortex, 1978. **14**: p. 234-244.
56. Fahn, S. and R. Elthon, *The Unified Parkinson's Disease Rating Scale.* Rec Dev in PD, 1987: p. 153-163.
57. Jankovic, J., et al., *Variable expression of Parkinson's disease: a baseline analysis of the DATATOP cohort.* Neurology, 1990. **40**: p. 1529-1534.
58. Langston, J., et al., *Core assessment program for intracerebral transplantations (CAPIT).* Mov. Disord., 1992. **7**: p. 2-13.
59. Dubbelink, K.O., et al., *Cognitive decline in Parkinson's disease is associated with slowing of resting-state brain activity: a longtitudinal study.* Neurobiology of Aging, 2013. **34**: p. 408-418.
60. Berendse, H. and C. Stam, *Stage-dependent patterns of disturbed neural synchrony in Parkinson's disease.* Parkinsonism and Related Disorders, 2007. **13**: p. S440-S445.
61. Sporns, O., *Networks of the Brain*. 2010.
62. Reus, M.d. and M.v.d. Heuvel, *Rich Club Organization and Intermodule Communication in the Cat Connectome.* Journal of Neuroscience, 2013. **33**(32): p. 12929-12939.
63. Heuvel, M.v.d. and O. Sporns, *Rich-Club Organization of the Human Connectome.* Journal of Neuroscience, 2011. **31**(44): p. 15775-15786.
64. Achard, S., et al., *A Resilient, Low-Frequency, Small-World Human Brain Functional Network with Highly Connected Association Cortical Hubs.* Journal of Neuroscience, 2006. **26**(2): p. 63-72.
65. Sporns, O. and C. Honey, *Identification and Classification of Hubs in Brain Networks.* PloS ONE, 2007. **2**(10): p. 1049.
66. Honey, C., et al., *Network structure of cerebral cortex shapes functional connectivity on multiple time scales.* PNAS, 2997. **104**(24): p. 10240-10245.
67. Bak, P., C. Tang, and K. Wiesenfeld, *Self-Organized Criticality: An Explanation of 1/f Noise.* Phys Rev Lett., 1987. **59**(4): p. 381-384.
68. Plenz, D. and T. Thiagarajan, *The organizing principles of neuronal avalanches: cell assemblies in the cortex?* TRENDS in Neurosciences, 2007. **30**(3): p. 101-110.
69. Pu, J., et al., *Developing neuronal networks: Self-organized criticality predicts the future.* Scientific Reports, 2013. **3**: p. 1-6.
70. Zare, M., M. Turalska, and P. Grigolini, *Phase transition and Self-Organized Criticality in the Brain*, in *APS March Meeting 2013*. 2013: Baltimore.
71. Beggs, J., *The criticality hypothesis: how local cortical networks might optimize information processing.* Phil. Trans. R. Soc. A, 2008. **366**: p. 329-343.
72. Meisel, C., et al., *Failure of Adaptive Self-Organized Criticality during Epileptic Seizure Attacks.* PLoS Comput Biol, 2012. **8**(1).
73. Mourik, A.v., A. Daffertshofer, and P. Beek, *Estimating Kramers-Moyal coefficients in short and non-stationary data sets.* Phys Lett A, 2006. **351**: p. 13-17.
74. Brede, M., *Locals vs. global synchronization in networks of non-identical Kuramoto oscillators.* Eur. Phys. J. B, 2008. **62**: p. 87-94.
75. Fox, M., et al., *The human brain is intrinsically organized into dynamic, anticorrelated functional networks.* PNAS, 2005. **102**(27): p. 9673-9678.
76. Hoehn, M. and M. Yahr, *Parkinsonism: onset, progression and mortality.* Neurology, 1967. **17**(5).
77. Marttila, R. and U. Rinne, *Disability and Progression in Parkinson's Disease.* Acta Neurologica Scandinavica, 1977. **56**(2): p. 159-169.
78. Stam, C., et al., *Graph theoretical analysis of mangetoencephalographic functional connectivity in Alzheimer's disease.* Brain, 2009. **132**: p. 213-224.
79. Collin, G., et al., *Impaired cerebellar functional connectivity in schizophrenia patients and their healthy siblings.* Frontiers in Psychiatry, 2011. **2**.
80. Stephan, K., T. Baldeweg, and K. Friston, *Synaptic Plasticity and Dysconnection in Schizophrenia.* Biol. Psychiatry, 2006. **56**: p. 929-939.
81. Shu, N., et al., *Diffusion Tensor Tractography Reveals Disrupted Topological Efficiency in White Matter Structural Networks in Multiple Sclerosis.* Cerebral Cortex, 2011. **21**: p. 2565-2577.
82. Hindriks, R., et al., *Data-Driven Modeling of Phase Interactions Between Spontaneous MEG Oscillations.* Human Brain Mapping, 2011. **32**: p. 1161-1178.
83. Wolters, E., T.v. Laar, and H. Berendse, *Parkinsonism and Related Disorders*. 2008.
84. Davie, C., *A review of Parkinson's disease.* British Medical Bulletin, 2008. **86**: p. 109-127.
85. Braak, H., et al., *Stages in the development of Parkinson's disease-related pathology.* Cell Tissue Res, 2004. **318**: p. 121-134.
86. Bosboom, J., et al., *Resting state oscillatory brain dynamics in Parkinson's disease: An MEG study.* Clinical Neurophysiology, 2006. **117**: p. 2521-2531.
87. Pfurtscheller, G. and F.L.d. Silva, *Event-related EEG/MEG synchronization and desynchronization: basic principles.* Clinical Neurophysiology, 1999. **110**(11): p. 1842-1857.

88.   Pfurtscheller, G., et al., *Post-movement beta synchronization in patients with Parkinson's disease.* J Clin Neurophysiol, 1998. **15**(3): p. 243-250.
89.   Defebvre, L., et al., *Spatiotemporal Study of Bereitschaftspotential and Event-Related Desynchronization During Voluntary Movement in Parkinson's Disease.* Brain Topography, 1994. **6**: p. 237-244.
90.   Wang, H., A. Lees, and P. Brown, *Impairment of EEG desynchronisation before and during movement and its relation to bradykinesia in Parkinson's disease.* J Neurol Neurosurg Psychiatry, 1999. **66**: p. 442-446.
91.   Heuvel, M.v.d., et al., *Functionally linked resting-state networks reflect the underlying structural connectivity architecture of the human brain.* Hum Brain Mapp, 2009. **30**(10): p. 3127-3141.
92.   Honey, C., et al., *Predicting human resting-state functional connectivity from structural connectivity.* PNAS, 2009. **106**(6): p. 2035-2040.
93.   Coopmans, F., and A. Daffertshofer. *On the evolution of Kuramoto's order parameter.*